# ANALYSIS OF COMPENSATED STRUCTURES IN PLANAR TRANSMISSION LINES USING THE FDTD METHOD INCORPORATING TRIANGULAR SUBCELLS

Zhewang Ma, Akira Miyata, and Eikichi Yamashita
The University of Electro-Communications
1-5-1 Chofugaoka, Chofu-shi, Tokyo 182, Japan

## ABSTRACT

A FDTD algorithm incorporating triangular subcells has been developed to implement dynamic analysis of compensated structures in planar transmission lines. Curvilinear or slanted metallic surfaces utilized in most compensated circuits are properly modeled by the use of triangular subcells, consequently, the numerical accuracy and computational efficiency are significantly improved. Characteristics of compensated microstrip right-angle bends, T-junctions, and meander lines are investigated, and discussions on the optimal compensation dimensioning rules are presented.

## INTRODUCTION

In the design of planar microwave and millimeter wave circuits, compensation of discontinuities is widely used in order to minimize the reactive and radiative effects [1]-[3]. For this reason, accurate characterization of compensated discontinuities in planar transmission line structures has been of significant importance, and substantial research efforts have been made in this area in the last two decades. Methods for characterizing compensated discontinuities of planar transmission line structures can be divided into three groups: (1) Quasi-static methods, in which equivalent capacitances and inductances associated with the discontinuities are evaluated. (2) Two-dimensional planar waveguide model approach. This approach is analytically easy and numerically efficient, but can only provide reliable results at low frequencies.
(3) Full-wave analysis, which is represented by integral equation methods and space discretization methods, like the finite-difference time-domain (FDTD) method.

A comparative review of past works on compensated discontinuities reveals that compensation of microstrip right-angle bends have received more attention than any other form of discontinuity. Moreover, while works by the quasi-static method and the planar waveguide model have discussed, to some extent, ways for realizing optimally compensated microstrip right-angle bends, the results are either empirically obtained through measurements or valid only in limited ranges of structural parameters and working frequencies [1]-[4]. On the other hand, most of the papers using full-wave methods addressed primarily analytical and numerical techniques for achieving minimum approximations and maximum accuracy and efficiency in the treatment of compensated discontinuities, and they contained little information concerning dimensioning rules for compensated structures [2]-[7]. As a result, when we try to employ compensated configurations for the high frequency design of planar transmission line circuits, we are still forced to resort to formulations and graphs obtained by quasi-static method or planar waveguide model, due to the lack of references on compensation effects obtained by full-wave analysis procedures.

The purpose of this paper includes two parts. First, a FDTD algorithm incorporating triangular subcells has been developed to carry out dynamic analysis of compensated discontinuities in planar transmission line structures. Second, compensation effects associated with a variety of discontinuities, such as microstrip right-angle bends, T-junctions, and meander lines, are investigated by using the developed FDTD algorithm. Where possible, comparisons with measured or theoretical values of other researchers are made, and the results are in good agreement with previous publications. Discussions on the optimal compensation dimensioning rules are presented, and special considerations are given to chamfered right-angle bends.

## THEORY

The FDTD method is employed in this work becaused of its versatility, accuracy and many other advantages [7]-[9]. However, one problem arises when it is applied to compensated discontinuities. Curvilinear or slanted metallic surfaces contained by most compensated discontinuities have to be approximated by staircases in the conventional FDTD algorithm using Yee cells [7][8]. Unfortunately, the staircase approximation of curved or slanted metal surfaces does not provide accurate results in many cases. Furthermore, it incurs additional computational costs like larger computer memories and longer computation times, due to the excessively fine meshes which must be used to model the discontinuities.

In this paper, a FDTD algorithm incorporating triangular subcells is developed for analyzing compensated discontinuities. In the analysis, while the spatial computational domain containing the subject under analysis is discretized by Yee's orthogonal grids, a curved or slanted metal boundary is approximated by a continuous chain of triangular subcells

This work is supported in part by the Grant-in-Aid for Scientific Research of the Ministry of Education, Science and Culture of Japan.



0-7803-3246-6/96/$5.00 © IEEE

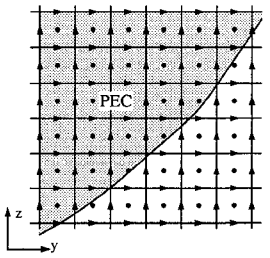


Figure 1: Triangular subcells for modeling a curved metal surface.

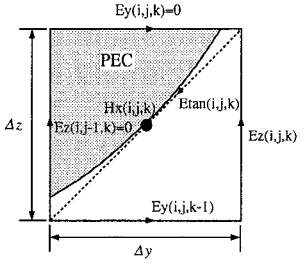


Figure 2: Field components at a triangular subcell.

as shown in Fig. 1. One of the enlarged triangular subcell is illustrated in Fig. 2, and the proper FDTD formulation for this cell is obtained from the integral form of Maxwell's equations [8][10].

$$\frac{\partial}{\partial t}\int\int \epsilon \boldsymbol{E}\cdot d\boldsymbol{s} = \oint \boldsymbol{H}\cdot d\boldsymbol{l} \tag{1}$$

$$\frac{\partial}{\partial t}\int\int \mu_0 \boldsymbol{H}\cdot d\boldsymbol{s} = -\oint \boldsymbol{E}\cdot d\boldsymbol{l} \tag{2}$$

Rewriting (2) at the triangular subcell, we have

$$\mu_0[H_x^{n+\frac{1}{2}}(i,j,k) - H_x^{n-\frac{1}{2}}(i,j,k)]\cdot\frac{\Delta y\Delta z}{2\Delta t} = -E_y^n(i,j,k-1)$$

$$\Delta y - E_z^n(i,j,k)\Delta z - E_{tan}^n(i,j,k)\sqrt{\Delta y^2+\Delta z^2} \tag{3}$$

where $\Delta y$, $\Delta z$, and $\Delta t$ are the increments in space and time domain respectively, $i$, $j$, and $k$ are the space coordinate indexes. $E_{tan}^n$ is the electric field component along the cell diagonal and can be considered as zero since it is quite close the metallic surface. Isolating $H_x^{n+\frac{1}{2}}(i,j,k)$ from (3) yields the time-stepping expression for the triangular subcell

$$H_x^{n+\frac{1}{2}}(i,j,k) = H_x^{n-\frac{1}{2}}(i,j,k)) + \frac{2\Delta t}{\mu_0\Delta z}[E_y^n(i,j,k) -$$

$$E_y^n(i,j,k-1)] - \frac{2\Delta t}{\mu_0\Delta y}[E_z^n(i,j,k) - E_z^n(i,j-1,k)] \tag{4}$$

We note that the formula for the same magnetic component at other rectangular cells is

$$H_x^{n+\frac{1}{2}}(i,j,k) = H_x^{n-\frac{1}{2}}(i,j,k)) + \frac{\Delta t}{\mu_0\Delta z}[E_y^n(i,j,k) -$$

$$E_y^n(i,j,k-1)] - \frac{\Delta t}{\mu_0\Delta y}[E_z^n(i,j,k) - E_z^n(i,j-1,k)] \tag{5}$$

Comparing (4) and (5), we see that the modified formula (4) for the triangular subcell differs from the normal one (5) only by the 2 factor in the right hand side. From the above process, it is seen that in the triangular subcells, all of the finite-difference expressions for updating the field components remain unvaried from those of the normal orthogonal Yee's algorithm, except the one for the magnetic field component located at the center of the triangular subcells, which is expressed by (4). Therefore, compared with the normal Yee's algorithm, only a little additional implementation effort is needed for the FDTD algorithm incorporating triangular subcells. However, as triangular subcells allow easier and better modeling of curvilinear and slanted parts of boundaries, the flexibility, accuracy, and computational efficiency are significantly improved.

## NUMERICAL RESULTS AND DISCUSSIONS

In order to validate our FDTD algorithm, we first calculated the scattering response of a microstrip right-angle bend. The width of the line is $w = 3$ mm, and the substrate parameters are $\varepsilon_r = 4.5$, and $h = 1.6$ mm. The results are shown in Fig. 3 by solid lines, and are compared with the dotted lines, which are the measured values of [7]. It is seen that our theoretical prediction agrees fairly well with the measurements. Resonances appearing in the measured results are attributed to the imperfection of the connector-strip junctions used in the experimental apparatus [7].

Compensation of a microstrip right-angle bend is usually realized by chamfering the outer portion of the corner, and the inset of Fig. 4(a) shows a 45° chamfered microstrip right-angle bend. The structural parameters of the microstrip line are $w = 0.6096$ mm, $h = 0.635$ mm, and $\varepsilon_r = 9.9$, with a characteristic impedance of 50 Ω. The compensation effects are investigated by calculating the scattering parameters of the bend with various amounts of chamfering, and the results are illustrated in Figs. 4(a) and (b). We observe that as the chamfering dimension $c/w$ increases from zero, the value of the reflection coefficient is reduced throughout the whole frequency range. When $c/w = 1.5$, $|S_{11}|$ is minimized, and the optimal compensation of the bend is obtained: the amplitude of $S_{11}$ is less than -35 dB at frequencies up to 19

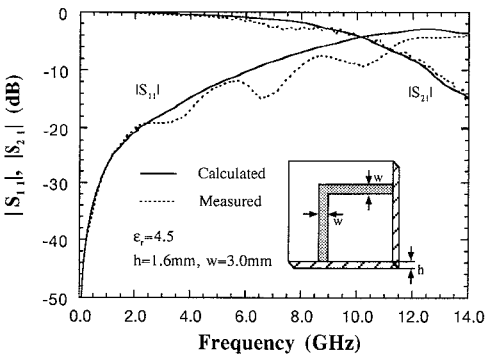


Figure 3: Comparison between calculated and measured values of scattering parameters of a microstrip right-angle bend.

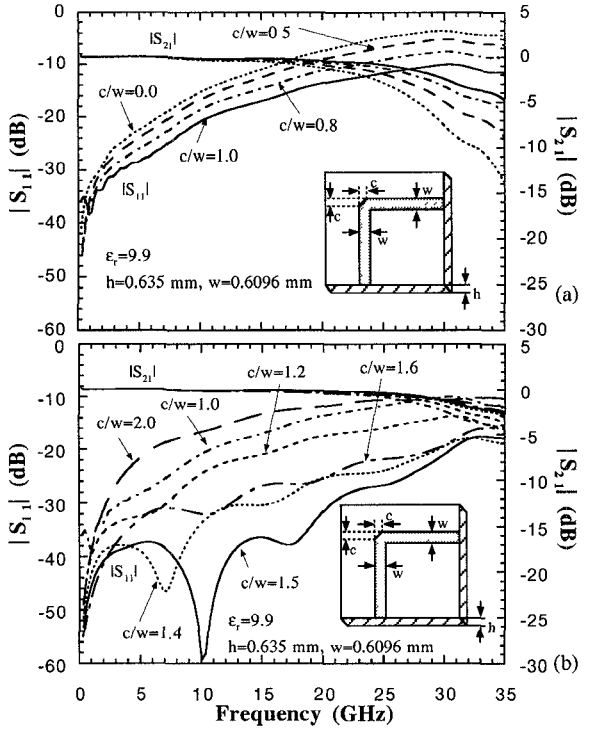


Figure 4: Variation of scattering parameters for a chamfered microstrip bend with various amounts of chamfering. (a) $0 \leq c/w \leq 1.0$, and (b) $1.0 \leq c/w \leq 2.0$.

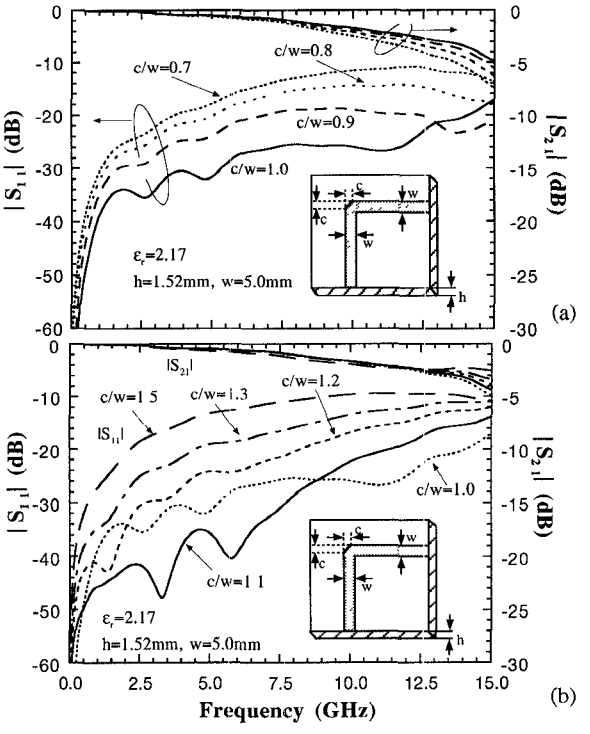


Figure 5: Variation of scattering parameters for a chamfered microstrip bend with various amounts of chamfering. (a) $0.7 \leq c/w \leq 1.0$, and (b) $1.0 \leq c/w \leq 1.5$.

GHz, and less than -20 dB up to 30 GHz. As the value of $c/w$ is increased from 1.5, the bend is overcompensated, and the reflection curves bounce back to higher levels.

Compensation of microstrip right-angle bend is further investigated by using another chamfered bend whose structural parameters are $w = 5$ mm, $h = 1.52$ mm, and $\varepsilon_r = 2.17$. The characteristic impedance of the line is also chosen as 50 $\Omega$. The results are shown in Figs. 5(a) and (b), and we observed similar variation in the behaviors of the reflection coefficient with respect to the chamfering dimension $c/w$. The optimal compensation is obtained at $c/w = 1.1$ this time, with the amplitude of $S_{11}$ less than -30 dB at frequencies lower than approximately 8 GHz.

We note that Douville and James [3] have made many measurements using microstrip right-angle bends with various amounts of chamfering. Based on the measured data, they produced empirical expressions for determining optimal chamfering of microstrip right-angle bends. When bends in lines with characteristic impedances of 50 $\Omega$ are considered, their expression for optimal chamfering dimension can be written as $c/w = (96 + 5\varepsilon_r)/100$, and this expression is expected valid for $1 \leq \varepsilon_r \leq 16$, and $0 < f \cdot h < 10$ GHz [1][3].

Substituting the structural parameters of the two bends discussed in Figs. 4 and 5 into the above formula, we get quasi-static estimation of the optimal chamfering dimensions for the two bends: The bend of Fig. 4 is optimally compensated at $c/w$ =1.42 in the frequency range $0 < f < 15.75$ GHz, and the bend of Fig. 5 at $c/w$ =1.03 between $0 < f <$ 6.5 GHz. On the other hand, dynamic curves in Figs. 4 and 5 indicate that the optimal chamfering ratio $c/w$ is 1.5 in the frequency range $0 < f < 31$ GHz for the bend of Fig. 4, and 1.1 between $0 < f < 9$ GHz for the bend of Fig. 5. This comparison reveals that optimal compensation dimensions of microstrip right-angle bends estimated by the above empirical formula are quite close to the ones obtained by FDTD analysis. Therefore, when optimal compensation is not critically required in the design of compensated right-angle bends, the empirical quasi-static formula can be used for convenience. In case accurate analysis and design over a wide frequency range are needed, the FDTD algorithm used in this paper provides a powerful tool.

Discontinuity reactance associated with a T-junction can be compensated by removing a portion from the junction, like a 45° isosceles triangle shown by the insets of Fig. 6. In Fig. 6(a), scattering parameters of a mitered and an unmitered T-junction are demonstrated, and they are compared with the measured and theoretical results of [5], all shown good agreement. In Fig. 6(b), variations in the behavior of the reflection coefficient $S_{33}$ at Port 3 are investigated with different sizes of the removed triangle. It is observed that the amplitude of $S_{33}$ is reduced as $c/w$ increases, and this improvement is particularly pronounced at higher frequencies.

Finally scattering characteristics of microstrip meander lines with and without chamfering of the bends are compared in Figs. 7(a) and 7(b). The configurations of the meander lines and their structural parameters are given by the insets

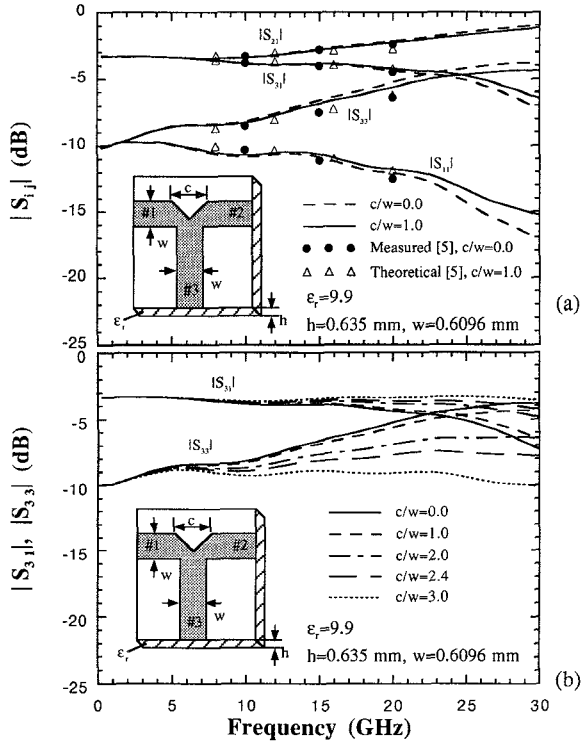


Figure 6: (a) Frequency dependence of the scattering parameters of a mitered and an unmitered T-junction. (b) Variation of the amplitudes of $S_{33}$ and $S_{31}$ with various amounts of mitering.

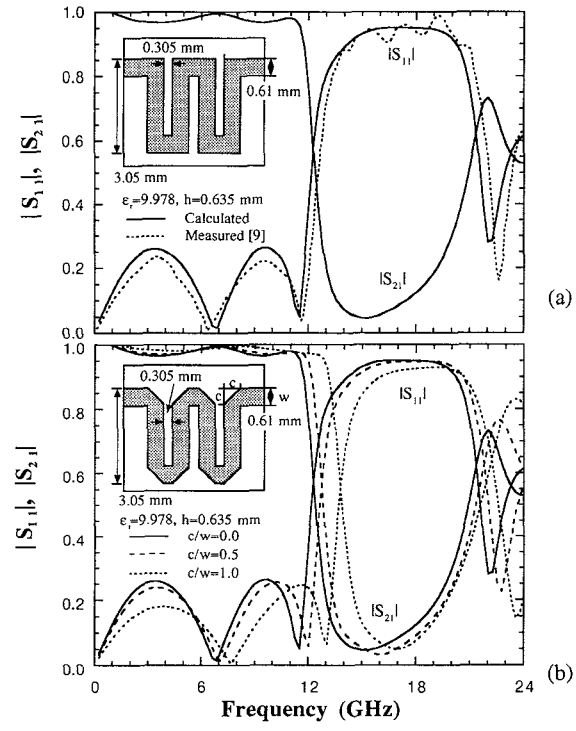


Figure 7: (a) Comparison between calculated and measured values of scattering parameters of a meander line, and (b) scattering parameters of meander lines with various amounts of chamfering on the corners.

of Fig. 7. In the case of the meander line without chamfering, shown in Fig. 7(a), good agreement between our calculated results and the measurements of [9] is seen. From the curves in Fig. 7(a), we see that scattering characteristics of the meander line are similar to those of a low-pass filter. In Fig. 7(b), influence of the chamfering of corners on the scattering parameters of a meander line is investigated. It is seen that with an increase of the chamfering dimension $c/w$, the bandwidth of the low-pass region is widened, and the amplitude of $S_{11}$ in this region is reduced. If the number of coupled U-bends in the meander line is increased, we expect that the effect of the chamfering on the scattering response will be more significant.

## ACKNOWLEDGMENT

The authors thank Professor Naoto Kishi of the University of Electro-Communications for his helpful discussions.

# References

[1] R. K. Hoffman, *Handbook of Microwave Integrated Circuits.* Norwood, MA: Artech House, 1987.

[2] T. Edwards, *Foundations for Microstrip Circuit Design*, 2nd ed. Chichester, U.K.: John Wiley & Sons, 1992.

[3] R. J. Douville and D. S. James, "Experimental study of symmetric microstrip bends and their compensation," *IEEE Trans. Microwave Theory Tech.*, vol. MTT-26, pp. 175-182, Mar. 1978.

[4] R. Chadha and K. C. Gupta, "Compensation of discontinuities in planar transmission lines," *IEEE Trans. Microwave Theory Tech.*, vol. MTT-30, pp. 2151-2156, Dec. 1982.

[5] T. S. Horng, W. E. McKinzie and N. G. Alexopoulos, "Full-wave spectral-domain analysis of compensation of microstrip discontinuities using triangular subdomain functions," *IEEE Trans. Microwave Theory Tech.*, vol. MTT-40, pp. 2137-2147, Dec. 1992.

[6] J. X. Zheng and D. C. Chang, "Numerical modeling of chamfered bends and other microstrip junctions of general shap in MMICS," *IEEE MTT-S Int. Microwave Symp. Dig.*, 1990, pp. 709-712.

[7] N. Feix, M. Lalande, and B. Jecko, "Harmonical characterization of a microstrip bend via the finite difference time domain method," *IEEE Trans. Microwave Theory Tech.*, vol. MTT-40, pp. 955-961, May 1992.

[8] A. Taflove, *Computational Electrodynamics. The Finite-Difference Time-Domain Method.* Norwood, MA: Artech House, 1995.

[9] A. Bahr, A. Lauer, and I. Wolff, "Application of the PML absorbing boundary condition to the FDTD analysis of microwave circuits," *IEEE MTT-S Int. Microwave Symp. Dig.*, 1995, pp. 27-30.

[10] P. Mezzanotte, L. Roselli, and R. Sorrentino, "A simple way to model curved metal boundaries in FDTD algorithm avoiding staircase approximation," *IEEE Microwave and Guided Wave Lett.*, vol. 5, pp. 267-269, Aug. 1995.